Research article

NMR IN BIOMEDICINE

Received: 13 October 2014, Revised: 17 February 2015, Accepted: 7 March 2015, Published online in Wiley Online Library: 29 April 2015

(wileyonlinelibrary.com) DOI: 10.1002/nbm.3295

Orotracheal administration of contrast agents: a new protocol for brain tumor targeting

Andrea Bianchi[a†], Damien Moncelet[a†], François Lux[b], Marie Plissonneau[b,c], Silvia Rizzitelli[a], Emeline Julie Ribot[a], Nawal Tassali[a], Véronique Bouchaud[a], Olivier Tillement[b], Pierre Voisin[a] and Yannick Crémillieux[a]*

The development of new non-invasive diagnostic and therapeutic approaches is of paramount importance in order to improve the outcome of patients with glioblastoma (GBM). In this work we investigated a completely non-invasive pre-clinical protocol to effectively target and detect brain tumors through the *orotracheal route*, using ultra-small nanoparticles (USRPs) and MRI.

A mouse model of GBM was developed. *In vivo* MRI acquisitions were performed before and after intravenous or orotracheal administration of the nanoparticles to identify and segment the tumor. The accumulation of the nanoparticles in neoplastic lesions was assessed *ex vivo* through fluorescence microscopy.

Before the administration of contrast agents, MR images allowed the identification of the presence of abnormal brain tissue in 73% of animals. After orotracheal or intravenous administration of USRPs, in *all* the mice an excellent co-localization of the position of the tumor with MRI and histology was observed. The elimination time of the USRPs from the tumor after the orotracheal administration was approximately 70% longer compared with intravenous injection.

MRI and USRPs were shown to be powerful imaging tools able to detect, quantify and longitudinally monitor the development of GBMs. The absence of ionizing radiation and high resolution of MRI, along with the complete non-invasiveness and good reproducibility of the proposed protocol, make this technique potentially translatable to humans. To our knowledge, this is the first time that the advantages of a *needle-free* orotracheal administration route have been demonstrated for the investigation of the pathomorphological changes due to GBMs. Copyright © 2015 John Wiley & Sons, Ltd.

Additional supporting information may be found in the online version of this article at the publisher's web site.

Keywords: glioblastoma; MRI; contrast agents; lungs; fluorescence imaging; orotracheal administration

INTRODUCTION

Glioblastoma (GBM) is the most common malignant primary brain tumor in adults. Despite conventional treatments, which typically include surgery, radiation, and cytotoxic chemotherapies, the median survival rate is only 14.6 months (1–3). These therapies show limits such as neurotoxicity, lack of specificity, and severe side effects. In addition, the blood–brain barrier (BBB) plays an important role in the GBM therapy. Indeed this barrier stops the accumulation of several drugs in the tumor, limiting the efficiency of the therapeutic compounds. Moreover, the poor prognosis of this pathology is also related to the late detection of GBM, which is often diagnosed in its latest stages (1–3). The development of new diagnostic and therapeutic approaches is therefore of paramount importance in order to improve the outcome of patients with GBM.

In this context, imaging techniques play a major role in early detection of diseases. They can provide early diagnostics and non-invasive longitudinal patient follow-ups, and help to prepare and guide radiotherapy or surgery. In particular, MRI displays a good resolution and excellent soft tissue contrast. Moreover, MRI is completely non-invasive for the patient because of the absence of ionizing radiation (4–7). For all these reasons, MRI is currently the gold standard for GBM diagnosis (8).

Development of contrast agents has been actively pursued to improve the potential of MRI in early detection of several pathologies (9,10). Nanoscale particles and carriers have already demonstrated effective applications in the diagnosis of diseases. In addition, some of these nanocompounds, commonly known as theranostic agents, have also shown efficient results in the therapy of these pathologies (4,11). Nanoparticles have been reported to be efficacious in anti-angiogenesis therapy (12),

* *Correspondence to: Yannick Crémillieux, Centre de Résonance Magnétique des Systèmes Biologiques, CNRS UMR 5536, Université Bordeaux Segalen, Bordeaux, France.*
E-mail: yannick.cremillieux@u-bordeaux.fr

a *A. Bianchi, D. Moncelet, S. Rizzitelli, E. J. Ribot, N. Tassali, V. Bouchaud, P. Voisin, Y. Crémillieux*
Centre de Résonance Magnétique des Systèmes Biologiques, CNRS UMR 5536, Université Bordeaux Segalen, Bordeaux, France

b *F. Lux, M. Plissonneau, O. Tillement*
Institut Lumière Matière, CNRS UMR 5306, Université Claude Bernard, Domaine Scientifique de La Doua, Villeurbanne, France

c *M. Plissonneau*
Nano-H SAS, Saint-Quentin Fallavier, France

† *These authors contributed equally.*

Abbreviations used: *GBM, glioblastoma; USRP, ultra-small rigid platform; BBB, blood–brain barrier; Cy, cyanine; i.t., intratracheal; i.v., intravenous; UTE, ultra-short echo time; ROI, region of interest; CNR, contrast-to-noise ratio; SNR, signal-to-noise ratio; PBS, phosphate buffered saline; SE, signal enhancement; PK, pharmacokinetics; EPR, enhanced permeability and retention; NSCLC, non-small-cell lung cancer.*

immunotherapy (13), and gene therapy of GBM (14). Nanoparticles with radiosensitization properties have also been shown to be able to strongly improve the prognosis of GBM when used in conjunction with radiotherapy (15–17).

In order to deliver a high dose of radiation in the neoplastic site, while sparing healthy surrounding tissues, nanoparticles must show very good accumulation in the tumor for a sufficient time. On the other hand, nanoparticles must be cleared from the body in a reasonable time in order to avoid potential toxic effects. It is therefore straightforward that the administration modality plays a fundamental role in determining the efficiency of the nanoparticles, directly influencing the bioavailability of the injected substance and its elimination pathways. Among the possible administration routes, the possibility of delivering drugs to the body through the lungs has been rediscovered in the last decade, since it appears as an efficient, effective, non-invasive, reliable, and simple administration method (18–21), easily translatable to clinical practice (22).

In this work we describe for the first time a non-invasive preclinical protocol to effectively target and detect brain tumors through the orotracheal route, using small nanoparticles and MRI. These small nanoparticles, hereafter referred to as ultrasmall rigid platforms (USRPs), were injected orotracheally into glioma-bearing mice. USRPs are sub-5 nm particles composed of gadolinium chelates covalently grafted to a polysiloxane matrix (17,23). A near-infrared fluorophore, cyanine (Cy) 5.5, was also grafted onto some of these nanoparticles (24). *In vivo* GBM signal enhancement (SE) and pharmacokinetics (PK) of orotracheal (intratracheal, i.t.) administration were measured against standard intravenous (i.v.) administration of the same number of USRPs.

EXPERIMENT

Nanoparticle synthesis and characterization

The Gd-DOTA-based nanoparticles were synthesized and characterized according to the previously described protocol (24,25). To perform *ex vivo* fluorescence microscopy, Cy 5.5, a near-infrared dye, was covalently grafted on the nanoparticles (24,25). Fluorescent USRPs are characterized by one Cy 5.5 grafted to every 1000 DOTA-Gd. Their longitudinal relaxivity r_1 is approximately 6 $mM^{-1}\,s^{-1}$ per gadolinium ion at 7 T (i.e. 60 $mM^{-1}\,s^{-1}$ per nanoparticle). Further details about the synthesis and the characterization can be found in the supporting information (with Figures S1–S3).

In vitro studies

Cell culture

Human GBM cell line U87-MG from the American Type Culture Collection (ATCC, LGC Standards, Middlesex, UK) was cultured in Dulbecco's modified Eagle's medium (DMEM, Gibco, Fisher Scientific, Illkirch, France) supplemented with 10% fetal calf serum (FCS, Gibco), in a humidified atmosphere with 5% CO_2 at 37 °C.

Flow cytometry and fluorescence microscopy

Uptake of USRPs by U87 cells was studied *in vitro* by flow cytometry and fluorescence microscopy.

For flow cytometry, 10^5 cells were seeded in 24 multiwell plates (Becton-Dickinson, Le Pont de Claix, France, 2 cm^2/well) for 24 h. Subsequently cells were incubated for 4 h with the fluorescent USRPs ($[Gd^{3+}] = 5$ mM). Then the medium was discarded and the cells were washed with Roswell Park Memorial Institute Medium (RPMI, Gibco). Thereafter cells were re-suspended in RPMI and analyzed by flow cytometry (Guava easyCyte flow cytometer–counter, Millipore, Billerica, MA, USA, λ_{ex} 638 nm, λ_{em} 661 nm).

For fluorescence microscopy, cells were seeded on glass coverslips for 24 h and incubated for 4 h with USRPs ($[Gd^{3+}] = 10$ mM). After three washes, the coverslips were mounted on glass slides and observed using a Zeiss Axiovert 200 microscope (Jena, Germany).

In vivo studies

Animals

Five-week-old female NMRI nude mice ($n = 34$), weighing 21.0 g ± 0.4 g, were purchased from Elevage Janvier (Le Genest, Saint Isle, France). Before the beginning of the experiment, animals were acclimatized in a temperature-controlled environment for one week. Facility rooms were maintained at constant temperature (25 °C), humidity (40–50% relative humidity), and 12 h light–dark illumination cycle. Access to food and tap water was available *ad libitum*. Experiments were carried out following the INSERM (Institut National de la Santé et de la Recherche Médicale) guidelines regarding animal welfare with approval of the Comité d'Ethique en Expérimentation Animale de Bordeaux.

Tumor implantation

U87 cells were implanted in the brain of the nude immunodeficient mice ($n = 27$) as previously described (26). Animals were left in the temperature- and humidity-controlled environment described above for 8 days. Four mice did not undergo the orthotopic implantation and were left as controls. After 8 days, *all* the xenotransplanted animals developed a tumor and underwent MRI investigation for high-resolution detection of the brain tumor lesions.

Imaging protocol

MR images with a 7 T spectrometer were acquired starting from day 8 up to day 15. Between two different administrations of contrast agent on the same mouse, at least two days without any handling was planned in order to allow a complete elimination of the previously administered contrast agents (24,25,27). After the last imaging point animals were sacrificed for histological analysis or *ex vivo* fluorescence microscopy.

In detail, the first group, composed of four tumor-bearing mice and two controls, was imaged with MRI at day 8 before and after receiving an i.v. administration of 200 μL of USRPs ($[Gd^{3+}] = 50$ mM). The same operation was repeated at day 15.

The second group, composed of six tumor-bearing mice and two controls, was imaged with MRI at day 8 after orotracheal administration of 50 μL of USRPs ($[Gd^{3+}] = 200$ mM). On a subgroup of three animals, the same operation was repeated at day 10. On the other subgroup of three animals, the same operation was repeated at day 15. The orotracheal administration was performed as described in References 24 and 27.

The third group, composed of four tumor-bearing mice, was imaged with MRI at day 8 before and after receiving an i.v. administration of 200 μL of USRPs ($[Gd^{3+}] = 50$ mM). This group of mice, in contrast to the first group, underwent MRI at day 10 before and after an *orotracheal* administration of 50 μL of USRPs ($[Gd^{3+}] = 200$ mM).

The fourth group, composed of two tumor-bearing mice, was imaged with MRI at day 8 after orotracheal administration of a 50 μL solution of NaCl 0.9% and at day 10 after i.v. administration of 200 μL of NaCl 0.9%.

The fifth group, composed of three tumor-bearing mice, was imaged with MRI at day 8 before and after receiving an i.v. administration of 200 μL of Dotarem® ($[Gd^{3+}] = 50$ mM) (Guerbet, Villepinte, France).

The sixth group, of three tumor-bearing mice, was imaged with MRI at day 8 before and after receiving an orotracheal administration of 50 μL of Dotarem® ($[Gd^{3+}] = 200$ mM) (Guerbet).

MRI

The images were acquired with a 7 T BioSpec 70/20 spectrometer (Bruker, Ettlingen, Germany), using a transmitter/receiver quadrature coil of 25 mm inner diameter (Bruker). Mice were placed prone in a custom-built plastic holder and kept anesthetized with 2.5% isoflurane in a mixture of N_2/O_2 (80:20) via facial mask. The body temperature was kept constant using warm circulating water and the respiratory cycle was monitored constantly using a pressure sensor placed on the abdomen.

The images of the brain were acquired with a 2D ultra-short echo time (UTE) sequence (804 directions–256 points, two averages). For each animal 10 axial slices of the brain of 1 mm thickness were acquired with a TE of 368 μs, FOV of 2 cm × 2 cm, TR of 140 ms and FA of 60°, for a total acquisition time of about 4 min. The same sequence was used to image lungs, increasing the number of averages to four and the field of view to 3 cm × 3 cm. Images were reconstructed with the ParaVision 5.1 software (Bruker). All the images were saved and analyzed with freeware medical image analysis software (MIPAV by NIH, Bethesda, MD, USA).

Image analysis

The presence and position of the tumor in MR images was assessed by two independent users for all the mice, according to a blinded procedure relative to animal implantation.

For each MR image, tumors were identified and regions of interest (ROIs) in the tumor and in the healthy brain tissues were manually segmented to measure the total average signal. The noise of the images was quantified as the standard deviation of the mean signal of an ROI selected in the image background and the signal-to-noise in the tumor was computed. The contrast-to-noise ratio (CNR) in each image was computed as the difference between the signal in the tumor and in the healthy tissue, normalized to the standard deviation of the image noise.

The PK of the USRPs contrast agent in the tumor region was studied according to the protocol already described in Reference 25.

Ex vivo studies

A subgroup ($n = 4$) of tumor-bearing mice was imaged with *ex vivo* fluorescence imaging and histology at day 8 after orotracheal administration of 50 μL of USRPs-Cy 5.5 ($[Gd^{3+}] = 200$ mM). A subgroup ($n = 4$) of tumor-bearing mice was imaged with *ex vivo* fluorescence imaging at day 8 after i.v. administration of 200 μL of USRPs ($[Gd^{3+}] = 50$ mM).

In detail, 30 min after the orotracheal or i.v. administration, mice were intracardially perfused with phosphate buffered saline (PBS) and fixed using paraformaldehyde (4%) in PBS. Brains were post-fixed for 24 h, and then cryoprotected using sucrose gradients (10%, 20% and 30% in PBS). Brains were frozen using liquid nitrogen vapor and stored at −80 °C.

Ex vivo fluorescence imaging

Thirty micrometer cryostat frontal sections were collected in cold cryoprotectant (50% PBS, 30% ethylene glycol and 20% glycerol) and stored at −20 °C. Sections were washed four times in PBS and mounted on SuperFrost Plus slides with VECTASHIELD mounting medium containing DAPI (Vector Labs, Malvern, PA, USA). Slides were analyzed using a Leica (Leica Microsystems Inc., Buffalo Grove, IL, USA) DM5500 B microscope.

Histologic evaluation

Thirty micrometer cryosections were cut, dried at 45 °C and fixed in 100% acetone for 10 min at room temperature. The sections were stained with hematoxylin and eosin using a standard protocol for histological assessment of cellular density and necrosis, and analyzed under a Leica DM5500 B microscope (2.5× and 10× magnification).

Statistical analysis

Comparison of CNR, SE, and tumor volumes between groups (i.v. USRPs, i.t. USRPs, i.v. Dotarem®) was performed using the Kruskal–Wallis test with Dunn's multiple comparison (non-parametric equivalent of the one-way ANOVA test). The paired non-parametric Wilcoxon test was used to evaluate the significance of changes in CNR, SE, and tumor volumes at two different time points. Significance was fixed at the 5% probability level. All analyses were performed using GraphPad Prism (GraphPad Software, La Jolla, CA, USA). All the data are presented as mean value ± standard error of the mean.

RESULTS

In vitro USRP uptake by U87 cells

The ability of U87 tumor cells to take up USRPs was characterized *in vitro*. Flow cytometry experiments demonstrated the USRP uptake by U87 cells (Supporting Information, Figure S4(a)). When cells were incubated with the nanoparticles, the mean fluorescent intensity increased from 10 to 70 A.U. Fluorescent microscopy suggested that USRPs may be internalized by U87 cells (Supporting Information, Figure S4(b)), as recently demonstrated in Reference (28).

Glioma detection and *in vivo* accumulation of USRPs

An orthotopic model of brain tumor morphologically similar to GBM was implemented in immunodeficient mice, inoculating U87 tumor cells intracranially into the striatum of the animals.

Before the administration of contrast agent, UTE MR images allowed the identification of the presence of abnormal brain tissue in a number of animals (~73%). Nonetheless, the contours of the carcinogenic formations were not easily identifiable (Fig. 1(a)).

After orotracheal or i.v. administration of USRPs, UTE MR images allowed the identification of the tumor in *all* the mice (Fig. 1(b), (c)). For all of them, a good co-localization of the position of the tumor between MRI and histology was observed. A representative image of the co-localization between MRI and histology is shown in the Supporting Information, Figure S5.

Comparison of SE and of CNR in the identified tumors after the administration of the contrast agent (Fig. 2) showed approximately halved values for the orotracheal (50 μL at 200 mmol/L

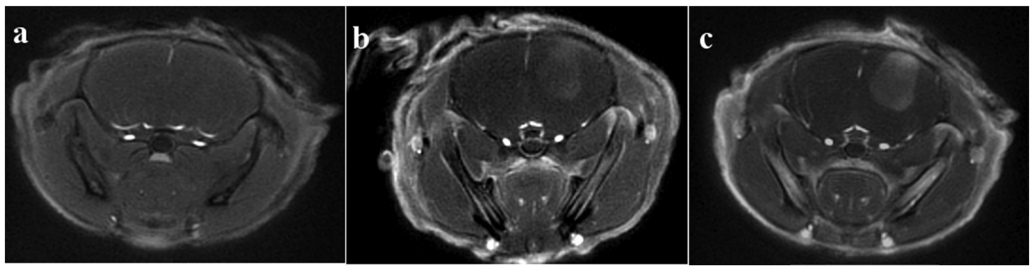

Figure 1. MR axial image of the brain (a) before and (b), (c) after the orotracheal (b) or i.v. (c) administration of the USRPs; (b) was acquired approximately 30 min after the orotracheal administration of 50 μL 200 mmol/L USRP [Gd^{3+}] whereas (c) was acquired approximately 30 min after the i.v. administration of 200 μL 50 mmol/L USRP [Gd^{3+}].

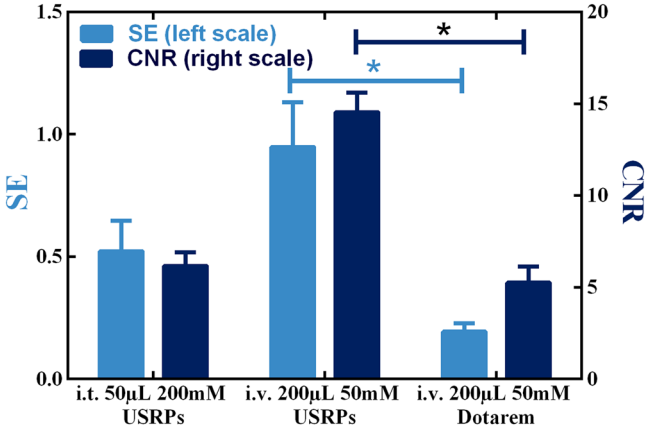

Figure 2. Bar plot showing the SE and CNR in tumors after the administration of the USRPs for the orotracheal (i.t., 50 μL at 200 mmol/L [Gd^{3+}]) and the i.v. route (i.v., 200 μL at 50 mmol/L [Gd^{3+}]), or after the i.v. administration of Dotarem® (i.v., 200 μL at 50 mmol/L [Gd^{3+}]), using the same amount of Gd^{3+}. Asterisks indicate significant differences ($p < 0.05$).

[Gd^{3+}]) administration with respect to the i.v. one (200 μL at 50 mmol/L [Gd^{3+}]), using the same amount of Gd^{3+}. The i.v. administration of a clinical commercially available contrast agent (Dotarem®) turned out to be approximately five times less effective than the same amount of intravenously administered USRPs (200 μL at 50 mmol/L [Gd^{3+}]). This latter observation is related to the high rigidity of the USRPs compared with commercially available contrast agents (r_1 per gadolinium ion at 7 T ~ 6 mM^{-1} s^{-1} versus r_1 Dotarem® at 7 T ~ 3 mM^{-1} s^{-1}) (29). Typically, an increase in the average signal-to-noise ratio (SNR) in brain tumor from 14.5 to 22.1, 28.3 and 17.3 was observed for the orotracheal administration of USRPs (50 μL at 200 mmol/L [Gd^{3+}]), the i.v. administration of USRPs (200 μL at 50 mmol/L [Gd^{3+}]), and the i.v. administration of Dotarem® (200 μL at 50 mmol/L [Gd^{3+}]), respectively. Similarly, an average increase of the CNR between tumor and healthy tissues from 2.1 to 6.2, 14.5, and 5.2 was observed for the orotracheal administration of USRPs (50 μL at 200 mmol/L [Gd^{3+}]), the i.v. administration of USRPs (200 μL at 50 mmol/L [Gd^{3+}]), and the i.v. administration of Dotarem® (200 μL at 50 mmol/L [Gd^{3+}]), respectively. No SE was observed after the orotracheal administration of Dotarem® (5.4 ± 6.2%).

The accumulation of the nanoparticles in the tumor region was assessed and confirmed by *ex vivo* fluorescence microscopy in a subgroup of animals, exploiting the multimodal potential of the USRPs. Cy 5.5 dye was covalently grafted onto the nanoassemblies and *ex vivo* microscopy was performed after the orotracheal or i.v. administration of the nanoparticles. Regardless of the administration modality, brain sections showed the nanoparticles' accumulation inside the tumor and poorly in the vicinity of the tumor (Fig. 3).

No SE of lung parenchyma or brain tumor was observed in tumor-bearing mice after i.v. or orotracheal administration of *saline* solution. Animals that were not inoculated with U87 cells were used as controls. No SE was observed in their brain after i.v. or orotracheal administration of contrast agent. On the other hand, homogeneous enhancements of their lung parenchyma were observed after orotracheal instillation (see References 24 and 27)

Pharmacokinetics data

The observed PK after orotracheal administration of contrast agents in the lungs of *healthy* animals reproduced the results observed in Reference 24, with fast diffusion of the nanoparticles in the lungs and slow but uniform elimination from the parenchymal tissue. The nanoparticles eliminated from the lungs passed into the bloodstream and were filtered by the kidneys. In all the animals a significant renal clearance and negligible hepatic elimination were observed, after orotracheal or i.v. administration, as already reported in References 24, 25, and 27. This phenomenon is mostly related to the ultra-small size of the nanoparticles (hydrodynamic diameter < 5 nm) (23-25,27,30,31). No accumulation in the brain was detectable with MRI for both the administration modalities in *healthy* mice due to unaltered BBB.

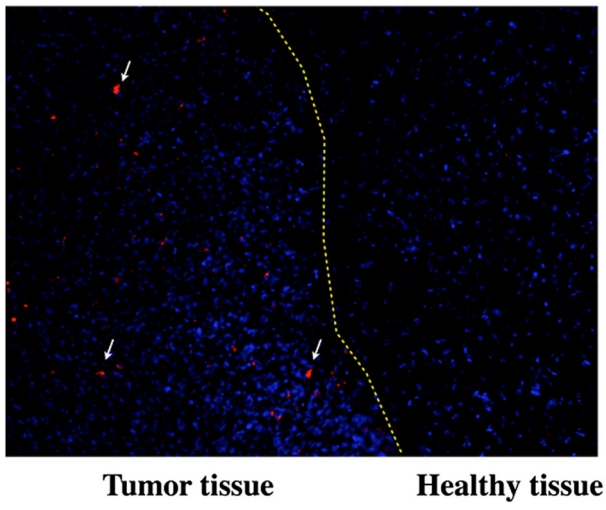

Figure 3. *Ex vivo* microscopy of a tumor section after i.t. administration of USRPs. White arrows indicate some fluorescent USRP-labeled cells inside the tumor.

In glioma-bearing mice, the PK observed in the tumor tissues after the i.v. administration of USRPs was rather different from that observed after orotracheal administration, as shown in Fig. 4. Following i.v. administration, the maximum SE of the tumor and CNR between tumor and healthy tissues were observed at the first acquired time point (5–10 min after injection). A rather fast elimination of the USRPs from the tumor tissue was then observed (50% drop of the SE observed in 28 ± 10 min).

On the other hand, the maximum of the SE was observed between 20 and 30 min after the orotracheal administration of USRPs. The elimination of the USRPs from the tumor after the orotracheal administration was approximately 70% longer compared with i.v. injection (50% drop of the SE observed in 46 ± 8 min). The CNR curve presented the same behavior as the SE one, indicating that the optimal time points for tumor detection and segmentation are between 20 and 30 min after the orotracheal administration.

Reproducibility of the protocol

A short-term reproducibility study for the orotracheal administration was performed. The subgroup of mice that received a second orotracheal administration of USRPs at 2 days interval showed no significant differences in tumor size ($p = 0.07$), SE ($p = 0.57$), or CNR ($p = 0.62$), confirming the reproducibility of the protocol (Supporting Information, Figure S6).

The possibility of studying the evolution of a tumor using the orotracheal administration protocol was evaluated. The subgroup of mice that received a second orotracheal administration of USRPs at 7 days interval showed a significant increase in the tumor volume quantified with MRI ($p < 0.01$). No significant increase in the SE ($p = 0.43$) or CNR ($p = 0.32$) was observed between the two time points (Supporting Information, Figure S7).

DISCUSSION

In the complex process of drug development, it is widely known that the administration route has a crucial role in the outcome of a given compound, since it affects, among other things, its bioavailability and its elimination (22,32). In the last two decades, strong interest has arisen around systemic delivery of therapeutic drugs through inhalation, a delivery path that proved to be a fast, effective, and above all non-invasive way to bring macromolecules or small molecules into the blood circulation before reaching the desired target (18,22). The most striking example of the clinical potential of this administration route can be found in the multiplication of the number of inhaled insulin formulations approved (in Europe and the USA) for the treatment of diabetic patients. It is worth mentioning that these inhaled drugs have been shown to be as reliable and safe as injected insulin (22,33–36).

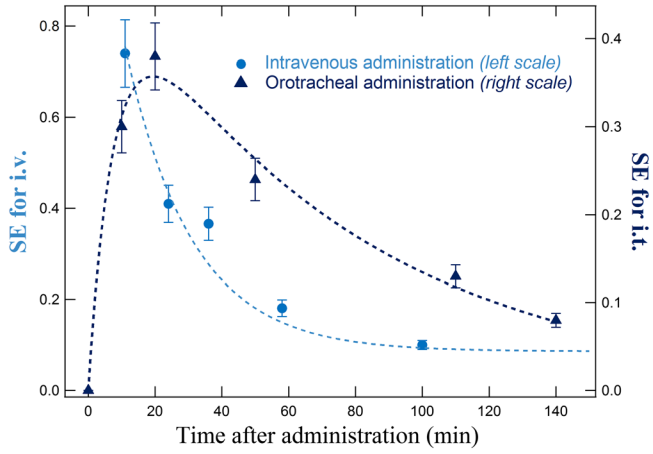

Figure 4. Plot showing the SE of the tumor as a function of time after i.v. or orotracheal administration. Dashed lines indicate the approximate PK behavior observed with the two administration routes (indicative fit of the data, not used for quantification).

Building on these promising developments and clinical applications, in this work we have decided to investigate the feasibility of using orotracheally delivered contrast agents in order to visualize and delineate GBM in a validated mouse model (26). To do so, previously studied gadolinium-based nanoparticles with high relaxivity and ultra-small size have been selected for the investigation (17,23–25,27). Orotracheal administration of USRPs was compared with a standard i.v. administration of the same contrast agent with respect to tumor SE, CNR, and PK.

Both the administration modalities allowed the visualization and delineation of the brain tumor volume, as confirmed by histological analysis. For both the routes, indeed, the tumor borders were easily identifiable after the administration of the same quantity of Gd^{3+}. The accumulation of the nanoparticles in the tumor tissues was confirmed by *ex vivo* fluorescence microscopy. It is important to mention here that, on average, only one nanoparticle in 100 presents a grafted fluorophore, implying that the fluorescence visible in the tumor region represents only a small percentage of the total significant accumulation (Fig. 3). No significant fluorescent USRPs were found in the healthy tissues surrounding the tumor. These findings are of crucial importance since, for the first time, they show that the orotracheal route is a viable non-invasive path to reach brain tumors, opening the way to a new fully non-invasive diagnostic approach to GBM.

The SNR and CNR values measured after i.v. administration were higher compared with those obtained for i.t. administration. This result is not surprising, considering that the orotracheal administration requires a further step compared with the i.v. route, i.e. the passage of the nanoparticles from the lungs to the blood system. These nanocompounds have indeed already been shown to be able to escape the lung mononuclear phagocytic system and pass rapidly from the airways to the bloodstream, before being finally filtered by the kidneys (24,25,27). This behavior is strongly related to the ultra-small hydrodynamic diameter of the nanoparticles and can be obtained with virtually any contrast agent having a diameter inferior to 6 nm. For higher hydrodynamic sizes, however, a variation of the trafficking of the particles across the alveolar surface into tissue and blood may be different (30) and the orotracheal route may no longer be effective for reaching brain tumors. Once in the blood, for both the i.t. and i.v. administrations, the contrast agents tend to accumulate in the brain tumor because of the BBB disruption and the consequent enabling of the well-known enhanced permeability and retention (EPR) effect (37,38). The USRPs are subsequently filtered by the kidney and excreted in the urine, without significant hepatic clearance.

This pharmacokinetic behavior of orotracheally administered nanoparticles should in principle also be valid for compounds such as Dotarem®. The fact that no SE of brain tumor was observed after orotracheal administration of Dotarem® is seemingly due to the lower relaxivity of this compound compared with the USRPs, as already observed in the fivefold lower SE measured

after i.v. administration of Dotarem®. In addition, a previous study has shown that Dotarem® has a brain tumor residence time about half that of the USRPs (39). As a consequence, the contrast is probably eliminated from the tumor before reaching a relevant concentration able to generate a visible enhancement of the GBM.

An increase in the concentration of the orotracheally administered Dotarem® would most probably result in a significant accumulation of the contrast agent in brain tissue, as observed for the USRPs.

The PKs observed after the two different administration modalities are different and reflect the distinct nanoparticle paths described above. For i.v. administrations, the maximum of the SE can be observed a few minutes after the administration of the contrast agent, due to the direct accumulation of the nanoparticles in the GBM because of passive targeting mechanisms. Nanoparticles are then quite rapidly cleared from the GBM and from the systemic circulation. This kind of PK presents the clear advantage of enabling a fast imaging protocol, which may be reflected in an effective patient management workflow in clinical practice. This administration route is the standard one for diagnostic applications nowadays.

In contrast, after orotracheal administration, a roughly homogeneous SE can be observed in the lung parenchyma. A slow but effective elimination of the contrast agent is then observed in the healthy lung tissue, with an elimination time constant of roughly two hours and a half. Once in the bloodstream, the nanoparticles are eliminated through the kidneys. If a brain tumor is present, the nanoparticle will accumulate in the neoplastic lesions because of the EPR effect, as schematically shown in Fig. 5. This protocol presents the inconvenient related to the fact that the maximum SE in the GBM is slightly delayed compared with i.v., potentially increasing (even though not dramatically) the time required for an examination in clinical practice. On the other hand, the protocol is non-invasive and does not require the use of needles.

The long residence time of the USRPs in the tumor permit us to envisage several imaging and therapeutic protocols. Ultra-small gadolinium-based nanoparticles, similar to the ones presented in this work, have been shown to have a potential theranostic application in brain tumors due to the radiosensitizing effect of the Gd atoms (15). The long retention of the USRPs in the tumor and the accurate knowledge of the PK of the contrast agent in the healthy and diseased tissues would allow tailoring of the radiation therapy according to the accumulation effect measurable with MRI. As a consequence, this would optimize the theranostic efficacy of these nanoassemblies, reducing the radiation dose to healthy tissues. It is worth mentioning here that the retention of these nanoparticles might be even more effective when exploiting active targeting ligands such as cRGD, which has already been satisfactorily grafted on similar nanoparticles in a different study (40). Such a hypothesis is currently under investigation. Finally, considering

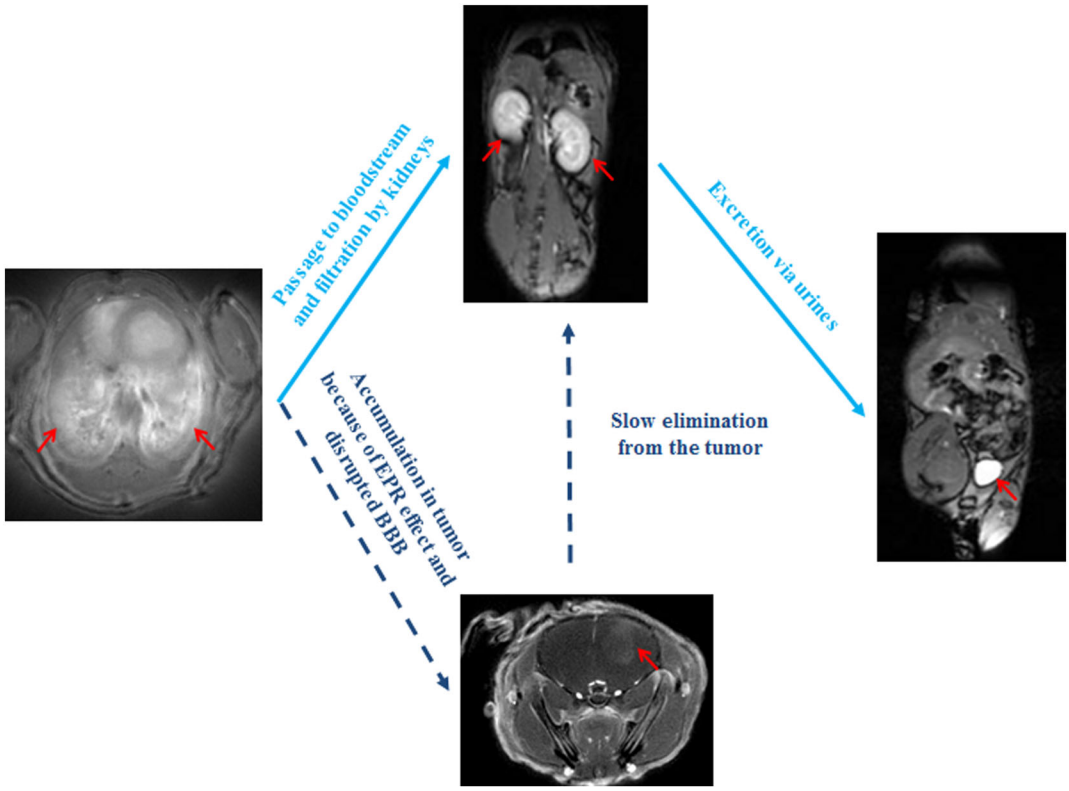

Figure 5. Schematic representation of accumulation and elimination pathways of orotracheally administered USRPs in healthy and glioma-bearing mice. The nanoparticles, administered directly to the lungs, enhance the signal of the pulmonary parenchyma in a homogeneous way. The contrast agents slowly pass to the bloodstream. Once there, two different pathways are possible: (i) in healthy mice, the USRPs are directly filtered by the kidneys and eliminated through the bladder without significant hepatic clearance (pathway schematically shown by solid lines); (ii) in glioma-bearing mice, some of the nanoparticles are directly filtered by the kidneys (as for healthy mice) while some of them tend to accumulate in the brain tumor because of the EPR effect. A slow elimination of the nanoparticles from the tumor site is subsequently observed, leading to the eventual elimination of the USRPs in the urine, without significant accumulation in the liver (pathway schematically shown by dashed lines). Arrows indicate the presence of the contrast agent in the lungs, kidneys, bladder, and brain tumor.

the long retention and rather specific accumulation of the nanoparticles in the neoplastic lesions, the possibility of using the USRPs as anti-cancer drug carriers is a concrete possibility that may be further explored in the future.

The orotracheal administration of contrast agents used in this animal study can be translated to humans with simple aerosols. Haage *et al*. (41) have indeed already shown that aerosolized gadolinium contrast agents can be safely administered to humans for lung applications. Leaving aside the possible implementation of theranostic treatments, it is important to mention that the protocol developed here does not require the use of needles, in contrast to i.v. administrations. This original non-invasive approach for diagnostics may have straightforward applications and advantages in clinical practice, considering that at least 10% of the population is affected by the pathological condition of needle phobia (42). This percentage most likely underestimates the real burden, since most of the patients suffering from this fear tend to avoid all medical treatments. Even for people not suffering from this real phobia, it is clear that a diagnostic protocol that uses aerosols instead of injections would be less traumatic for the patient and would most probably reduce the typical pre-examination stress. Nevertheless, it is important to underline here that this study is a proof of concept and thus further investigations will be needed to validate the inhalation route as a viable, safe and useful way of administering contrast agents to non-invasively diagnose GBMs in patients.

When measured only two days after orotracheal administration of USRPs, the brain tumors were statistically identical (SE, CNR, volume), confirming the reproducibility of the non-invasive measurements made with the proposed method. In addition, as expected, when measured at a one week interval, the non-treated carcinogenic formations increased in size and in tumor cell density. No increase in CNR or SE was observed, probably due to the fact that tumors take up roughly the same number of nanoparticles at the two different stages, as already observed for non-small-cell lung cancers (NSCLCs) (25).

T_2-weighted and T_1-weighted spin-echo sequences are usually employed for contrast-enhanced MRI visualization of mouse glioma (43) since these sequences provide high tumor tissue contrast in both pre- and post-contrast agent administration. In this work, the localization and delineation of brain tumors using both the orotracheal and the i.v. delivery of contrast agents was performed using an optimized UTE MRI sequence employing radial *k*-space sampling. The rationale behind this choice was twofold. First, the employed sequence is strongly T_1 weighted (27,44) with negligible T_2 weighting, thus allowing more accurate visualization of the contrast agent accumulation, distribution, and evolution. Second, the UTE sequence used in this study had been previously optimized to visualize lung parenchyma and pulmonary signal changes (24,25,27,45). These sequences are indeed less sensitive to cardio-respiratory motion than Cartesian MR acquisitions (45–48). As a consequence, free-breathing acquisitions can be performed with limited impact on lung image SNR, sharpness, and spatial resolution when the visualization of lung is of interest (45–48). In other words, the use of UTE sequences allowed at the same time the proper visualization of brain tumor SEs due to contrast agents and the visualization of the nanoparticles in the lungs when administered orotracheally.

In addition, the same MRI protocol with orotracheally administered nanoparticles as employed in this work has already been shown to be extremely efficient for the detection (25) and therapy (49) of NSCLCs. Knowing that the development of brain cancer metastasis may start from primary NSCLCs (50–52), the UTE protocol described in this work (in conjunction with contrast agents) may be employed for the simultaneous diagnosis and follow-up of both the organs.

In general, it is clear that the results presented in this work are fairly independent of the particular choice of the sequence, as long as the employed MRI pulse sequence is sensitive enough to detect changes in NMR brain signal related to the accumulation of a positive contrast agent. Nonetheless, even better results (higher SEs) may be achieved using spin-echo sequences.

In conclusion, the observed high reproducibility and efficacy of the protocol, altogether, make the orotracheal administration of Gd-based nanoparticles a good candidate for early brain cancer detection and non-invasive follow-up of this disease. In addition, the previously demonstrated negligible acute toxicity of the USRPs and favorable PK (24), their theranostic properties (15), and the possibility of replacing the orotracheal administration with a simpler aerosol, altogether, make the proposed protocol potentially translatable to human studies. To our knowledge, this is the first time that a study has clearly shown that the synergic employment of a T_1-weighted MRI UTE sequence and orotracheally administered gadolinium-based nanoparticles allow the detection of millimetric-size brain tumors and of their contours. This study has indeed shown that the orotracheal route is a viable pathway of strong interest to reach the brain, opening the way to the implementation of effective non-invasive and non-traumatic (needle-free) diagnostic protocols of brain tumor. Potential applications of this result may range from brain neoplastic pathology detection to therapeutic applications of selected drugs or lead compounds, grafted onto the contrast agent and non-invasively delivered to the tumor site through inhalation.

Conflict of Interest

The authors have no conflict of interest to declare.

Acknowledgements

A.B. acknowledges a fellowship from the European Network PINET (FP7-PEOPLE-2010-ITN-264864). The authors acknowledge the support of the Agence Nationale de la Recherche (ANR-12-P2N-0009) for the ANR project GD-LUNG. The authors acknowledge Mr Stephane Sanchez for help with the animals, Mr Gerard Raffard for help with the MRI, and Dr J. P. Konsman for help with histology.

REFERENCES

1. Stupp R, Mason WP, van den Bent MJ, Weller M, Fisher B, Taphoorn MJ, Belanger K, Brandes AA, Marosi C, Bogdahn U, Curschmann J, Janzer RC, Ludwin SK, Gorlia T, Allgeier A, Lacombe D, Cairncross JG, Eisenhauer E. Mirimanoff RO, for the European Organisation for Research and Treatment of Cancer Brain Tumor and Radiotherapy Groups and the National Cancer Institute of Canada Clinical Trials Group. Radiotherapy plus concomitant and adjuvant temozolomide for glioblastoma. N. Engl. J. Med. 2005; 352: 987–996.
2. Curran WJ, Jr, Scott CB, Horton J, Nelson JS, Weinstein AS, Fischbach AJ, Chang CH, Rotman M, Asbell SO, Krisch RE, Nelson DF. Recursive partitioning analysis of prognostic factors in three Radiation Therapy Oncology Group malignant glioma trials. J. Natl. Cancer Inst. 1993; 85: 704–710.
3. De Angelis LM. Brain tumors. N. Engl. J. Med. 2001; 344: 114–123.
4. Van Echteld CJA, Beckmann N. A view on imaging in drug research and development for respiratory diseases. J. Pharmacol. Exp. Ther. 2011; 337: 335–349.

5. Bernstein MA, King KF, Zhou XJ. *Handbook of MRI Pulse Sequences*. Elsevier: Burlington, VT; 2004.
6. Weissleder R, Pittet MJ. Imaging in the era of molecular oncology. Nature 2008; 452: 580–589.
7. Edelman RR, Hesselink JR, Zlatkin MB, Crues JV, III. *Clinical Magnetic Resonance Imaging*. Saunders–Elsevier: Philadelphia, PA; 2005.
8. Dhermain FG, Hau P, Lanfermann H, Jacobs AH, van den Bent MJ. Advanced MRI and PET imaging for assessment of treatment response in patients with gliomas. Lancet Neurol. 2010; 9: 906–920.
9. V. M. Runge. *Clinical MRI*. Saunders: Philadelphia, PA; 2002.
10. Merbach AE, Toth E, *The Chemistry of Contrast Agents in Medical Magnetic Resonance Imaging*. Wiley: New York; 2001.
11. Ferrari M. Cancer nanotechnology: opportunities and challenges. Nat. Rev. Cancer 2005; 5: 161–171.
12. Wojton J, Chu Z, Mathsyaraja H, Meisen WH, Denton N, Kwon CH, Chow LM, Palascak M, Franco R, Bourdeau T, Thornton S, Ostrowski MC, Kaur B, Qi X. Systemic delivery of SapC-DOPS has antiangiogenic and antitumor effects against glioblastoma. Mol. Ther. 2013; 21: 1517–1525.
13. Zhao D, Alizadeh D, Zhang L, Liu W, Farrukh O, Manuel E, Diamond DJ, Badie B. Carbon nanotubes enhance CpG uptake and potentiate antiglioma immunity. Clin. Cancer Res. 2011; 17: 771–782.
14. Kato T, Natsume A, Toda H, Iwamizu H, Sugita T, Hachisu R, Watanabe R, Yuki K, Motomura K, Bankiewicz K, Wakabayashi T. Efficient delivery of liposome-mediated MGMT-siRNA reinforces the cytotoxicity of temozolomide in GBM-initiating cells. Gene Ther. 2010; 17: 1363–1371.
15. Le Duc G, Miladi I, Alric C, Mowat P, Bräuer-Krisch E, Bouchet A, Khalil E, Billotey C, Janier M, Lux F, Epicier T, Perriat P, Roux S, Tillement O. Toward an image-guided microbeam radiation therapy using gadolinium-based nanoparticles. ACS Nano 2011; 5: 9566–9574.
16. Joh DY, Sun L, Stangl M, Al Zaki A, Murty S, Santoiemma PP, Davis JJ, Baumann BC, Alonso-Basanta M, Bhang D, Kao GD, Tsourkas A, Dorse JF. Selective targeting of brain tumors with gold nanoparticle-induced radiosensitization. PLoS One 2013; 8: e62425.
17. Mignot A, Truillet C, Lux F, Sancey L, Louis C, Denat F, Boschetti F, Bocher L, Gloter A, Stéphan O, Antoine R, Dugourd P, Luneau D, Novitchi G, Figueiredo LC, de Morais PC, Bonneviot L, Albela B, Ribot F, Van Lokeren L, Déchamps-Olivier I, Chuburu F, Lemercier G, Villiers C, Marche PN, Le Duc G, Roux S, Tillement O, Perriat P. A top-down synthesis route to ultrasmall multifunctional Gd-based nanoparticles for theranostic applications. Chem. Eur. J. 2013; 19: 6122–6136.
18. Patton JS, Fishburn CS, Weers JG. The lungs as a portal of entry for systemic drug delivery. Proc. Am. Thorac. Soc. 2004; 1: 338–344.
19. Driscoll KE, Costa DL, Hatch G, Henderson R, Oberdorster G, Salem H, Schlesinger RB. Intratracheal instillation as an exposure technique for the evaluation of respiratory tract toxicity: uses and limitations. Toxicol. Sci. 2000; 55: 24–35.
20. Costa DL, Lehmann JR, Winsett D, Richards J, Ledbetter AD, Dreher KL. Comparative pulmonary toxicological assessment of oil combustion particles following inhalation or instillation exposure. Toxicol. Sci. 2006; 91: 237–246.
21. Shoyele SA, Cawthome S. Particle engineering techniques for inhaled biopharmaceuticals. Adv. Drug Deliver. Rev. 2006; 58: 1009–1029.
22. Patton JS, Byron PR. Inhaling medicines: delivering drugs to the body through the lungs. Nat. Rev. Drug Discov. 2007; 6: 67–74.
23. Lux F, Mignot A, Mowat P, Louis C, Dufort S, Bernhard C, Denat F, Boschetti F, Brunet C, Antoine R, Dugourd P, Laurent S, Vander Elst L, Muller R, Sancey L, Josserand V, Coll JL, Stupar V, Barbier E, Rémy C, Broisat A, Ghezzi C, Le Duc G, Roux S, Perriat P, Tillement O. Ultra-small rigid particles as multimodal probes for medical applications. Angew. Chem. Int. Ed. Engl. 2011; 123: 12507–12511.
24. Bianchi B, Dufort S, Lux F, Courtois A, Tillement O, Coll JL, Crémillieux Y. Quantitative biodistribution and pharmacokinetics of theranostic multimodal gadolinium-based nanoparticles for lungs using ultra-short TE MRI. Magn. Reson. Mater. Phys. 2014; 27: 303–316.
25. Bianchi A, Dufort S, Lux F, Fortin PY, Tassali N, Tillement O, Coll JL, Crémillieux Y. Targeting and in vivo imaging of non-small-cell lung cancer using nebulized multimodal contrast agents. Proc. Natl. Acad. Sci. U. S. A. 2014; 111: 9247–9252.
26. Ribot EJ, Miraux S, Konsman JP, Bouchaud V, Pourtau L, Delville MH, Franconi JM, Thiaudière E, Voisin PJ. In vivo MR tracking of therapeutic microglia to a human glioma model. NMR Biomed. 2011; 24: 1361–1368.
27. Bianchi A, Lux F, Tillement O, Crémillieux Y. Contrast enhanced lung MRI in mice using ultra-short echo time radial imaging and intratracheally administrated Gd-DOTA-based nanoparticles. Magn. Reson. Med. 2013; 70: 1419–1426.
28. Stefančíková L, Porcel E, Eustache P, Li S, Salado D, Marco S, Guerquin-Kern JL, Réfrégiers M, Tillement O, Lux F, Lacombe S. Cell localization of gadolinium-based nanoparticles and related radiosensitising efficacy in glioblastoma cells. Cancer Nanotechnol. 2014; 5: 6.
29. Laurent S, Elst LV, Muller RN. Comparative study of the physicochemical properties of six clinical low molecular weight gadolinium contrast agents. Contrast Media Mol. Imaging 2006; 1: 128–137.
30. Choi HS, Ashitate Y, Lee JH, Kim SH, Matsui A, Insin N, Bawendi MG, Semmler-Behnke M, Frangioni JV, Tsuda A. Rapid translocation of nanoparticles from the lung airspaces to the body. Nat. Biotechnol. 2010; 28: 1300–1303.
31. Choi HS, Liu W, Liu F, Nasr K, Misra P, Bawendi MG, Frangioni JV. Design considerations for tumour-targeted nanoparticles. Nat. Nanotechnol. 2010; 5: 42–47.
32. Roa WH, Azarmi S, Al-Hallak MK, Finlay WH, Magliocco AM, Löbenberg R. Inhalable nanoparticles, a non-invasive approach to treat lung cancer in a mouse model. J. Control. Release 2011; 150: 49–55.
33. Patton JS, Bukar JG, Eldon MA. Clinical pharmacokinetics and pharmacodynamics of inhaled insulin. Clin. Pharmacokinet. 2004; 43: 781–801.
34. Quattrin T, Belanger A, Bohannon NJV, Schwartz SL. Efficacy and safety of inhaled insulin (Exubera) compared with subcutaneous insulin therapy in patients with type 1 diabetes: results of a 6-month, randomized, comparative trial. Diabetes Care 2004; 27: 2622–2627.
35. Hollander PA, Blonde L, Rowe R, Mehta AE, Milburn JL, Hershon KS, Chiasson JL, Levin SR. Efficacy and safety of inhaled insulin (Exubera) compared with subcutaneous insulin therapy in patients with type 2 diabetes: results of a 6-month, randomized, comparative trial. Diabetes Care 2004; 27: 2356–2362.
36. DeFronzo RA, Bergenstal RM, Cefalu WT, Pullman J, Lerman S, Bode BW, Phillips LS, Exubera Phase III. Study Group. Efficacy of inhaled insulin in patients with type 2 diabetes not controlled with diet and exercise: a 12-week, randomized, comparative trial. Diabetes Care 2005; 28: 1922–1928.
37. Maeda H, Wu J, Sawa T, Matsumura Y, Hori K. Tumor vascular permeability and the EPR effect in macromolecular therapeutics: a review. J. Control. Release 2000; 65: 271–284.
38. Matsumura Y, Maeda H. A new concept for macromolecular therapeutics in cancer chemotherapy: mechanism of tumoritropic accumulation of proteins and the antitumor agent smancs. Cancer Res. 1986; 46: 6387–6392.
39. Le Duc G, Roux S, Tuarez AP, Dufort S, Brauer E, Marais A, Truillet C, Sancey L, Perriat P, Lux F, Tillement O. Advantages of gadolinium based ultrasmall nanoparticles vs molecular gadolinium chelates for radiotherapy guided by MRI for glioma treatment. Cancer Nanotechnol. 2014; 5: 4.
40. Morlieras J, Dufort S, Sancey L, Truillet C, Mignot A, Rossetti F, Dentamaro M, Laurent S, Vander Elst L, Muller RN, Antoine R, Dugourd P, Roux S, Perriat P, Lux F, Coll JL, Tillement O. Functionalization of small rigid platforms with cyclic RGD peptides for targeting tumors overexpressing αvβ3-integrins. Bioconjugate Chem. 2013; 24: 1584–1597.
41. Haage P, Karaagac S, Spüntrup E, Truong HT, Schmidt T, Günther RW. Feasibility of pulmonary ventilation visualization with aerosolized magnetic resonance contrast media. Invest. Radiol. 2005; 40: 85–88.
42. Hamilton JG. Needle phobia: a neglected diagnosis. J. Fam. Pract. 1995; 41: 169–175.
43. Cha S, Johnson G, Wadghiri YZ, Jin O, Babb J, Zagzag D, Turnbull DH. Dynamic, contrast-enhanced perfusion MRI in mouse gliomas: correlation with histopathology. Magn. Reson. Med. 2003; 49: 848–855.
44. Crémillieux Y, Briguet A, Deguin A. Projection-reconstruction methods: fast imaging sequences and data processing. Magn. Reson. Med. 1994; 32: 23–32.
45. Bianchi A, Ozier A, Ousova O, Raffard G, Crémillieux Y. Ultrashort-TE MRI longitudinal study and characterization of a chronic model of asthma in mice: inflammation and bronchial remodeling assessment. NMR Biomed. 2013; 26: 1451–1459.
46. Zurek M, Bessaad A, Cieslar K, Crémillieux Y. Validation of simple and robust protocols for high-resolution lung proton MRI in mice. Magn. Reson. Med. 2010; 64: 401–407.

47. Bergin CJ, Pauly JM, Macovski A. Lung parenchyma: projection reconstruction MR imaging. Radiology 1991; 179: 777–781.
48. Bianchi A, Dufort S, Fortin PY, Lux F, Raffard G, Tassali N, Tillement O, Coll JL, Crémillieux Y. *In vivo* MRI for effective non-invasive detection and follow-up of an orthotopic mouse model of lung cancer. NMR Biomed. 2014; 27: 971–979.
49. Dufort S, Bianchi A, Henry M, Lux F, Le Duc G, Josserand V, Louis C, Perriat P, Crémillieux Y, Tillement O, Coll JL. Nebulized gadolinium-based nanoparticles: a theranostic approach for lung tumor imaging and radiosensitization. Small 2015; 11: 215–221.
50. Mintz A, Perry J, Spithoff K, Chambers A, Laperriere N. Management of single brain metastasis: a practice guideline. Curr. Oncol. 2007; 14: 131–143.
51. Eichler AF, Loeffler JS. Multidisciplinary management of brain metastases. Oncologist 2007; 12: 884–898.
52. Langer CJ, Mehta MP. Current management of brain metastases, with a focus on systemic options. J. Clin. Oncol. 2005; 23: 6207–6219.

SUPPORTING INFORMATION

Additional supporting information may be found in the online version of this article at the publisher's web site.